International Journal of Concrete Structures and Materials

RESEARCH

Open Access

Experimental Study on Dynamic Tensile Properties of Macro-Polypropylene Fiber Reinforced Cementitious Composites

Guoliang Yang, Jingjiu Bi*, Zhiwen Dong, Ying Li and Yi Liu

Abstract

Using a high-speed photography system and a split Hopkinson pressure bar, macro-polypropylene fiber reinforced cementitious composites are tested to reveal the effects of the macro-polypropylene fiber volume fraction and loading rate on the dynamic tensile strength and failure mode. We also analyze the functional relationship between the dynamic tensile strength, loading rate, and fiber volume fraction, and study the splitting failure process using digital image correlation technology. The evolution law of the strain and displacement fields of the specimens is obtained, and the effect of the fiber volume fraction on the crack initiation strain value is quantitatively studied. The results show that the appropriate fiber content (1.5–2%) can significantly improve the dynamic tensile strength, while a higher fiber content (2.5%) leads to deterioration of the specimen. Adding macro-polypropylene fiber prevents the specimen from undergoing central tensile fracturing under dynamic loading, and distributes the impact load more evenly, thus improving the ability of the specimen to resist cracking.

Keywords: Polypropylene fiber, Fiber cement-based material, Fiber volume fraction, Dynamic tensile strength, Digital image correlation method

1 Introduction

Cementitious composites have poor toughness and poor deformation ability. As a result, it is difficult for such composites to absorb energy through deformation under impact loading. This produces many disadvantages when applied to protection engineering. Adding fibers to cementitious composites can improve their tensile strength, ductility, toughness, and impact resistance (Konstantinos & P. SJ, 2021; Pakravan et al., 2017). Common fibers include metal, polymer, or natural fibers. In particular, polypropylene fibers have the advantages of high durability, light weight, and low cost, and when added to cementitious composites, they have the effect of strengthening and toughening the material. Hence, they are widely used in the field of protective engineering.

At present, the research on polypropylene fiber cementitious composites mostly focuses on micro-polypropylene fibers. The addition of fine fibers is greatly affected by fiber dispersion, and high dosages degrade the performance of the cementitious composites (MAZAHERIPOUR et al., 2010). Macro-polypropylene fibers (diameter is greater than 0.1 mm) achieve sufficient reinforcing and toughening effects to be considered as reliable substitutes for steel fibers (Yin, 2015), and can overcome the influence of fiber dispersion within a certain range. Hsie (Hsie et al., 2008) conducted an experimental study on the compressive and tensile strength of concrete samples containing fine and coarse polypropylene fibers. With the addition of coarse fibers, the strength of the material was significantly improved. Through experimental research, Liang (Liang et al., 2022) found that macro-polypropylene fiber reinforced cementitious composites (macro-PPFRCCs)

Journal information: ISSN 1976-0485 / eISSN2234-1315.

*Correspondence: sqt1700602039@student.cumtb.edu.cn; bijingjiu@126.com

School of Mechanics and Civil Engineering, China University of Mining and Technology-Beijing, Beijing 100083, China

can significantly improve the failure mode of the material. The bonding effect of macro-PPFRCCs also means that the material failure process presents excellent toughness characteristics.

Protective structures often face the threat of shock loads, such as from explosions, so it is necessary to conduct in-depth research on the dynamic mechanical properties of fiber–cement composites. Ye (Zhong, 2018) studied the dynamic compressive properties of steel fiber reinforced concrete under different fiber contents and strain rates, and found that an increase in the strain rate and fiber content significantly increased the strength of the samples. Xie (Xie et al., 2022) studied the dynamic tensile properties of basalt fiber reinforced concrete, and reported that the fracture time of the specimens was extended following the addition of basalt fibers. According to previous research (Enrico et al., 2021; Guo et al., 2019; Liang et al., 2018), the strain rate is an important factor affecting the dynamic mechanical properties of cement-based materials, which makes the study of material properties under dynamic loading more complicated than static tests. At present, the split Hopkinson pressure bar (SHPB) is the main device for studying the destruction mechanism of materials under dynamic loads (Zhou, 2011). However, it is difficult to determine the dynamic tensile failure process of the material accurately using an SHPB, so it is necessary to use more effective testing methods. Digital image correlation (DIC) is a non-destructive testing technology that can detect and analyze the strain field and displacement field during the fracture process of the specimen (Niu et al., 2019; Qing et al., 2019; Yu, 2018). Zhao (Zhao et al., 2018) studied the impact resistance of steel fiber reinforced cement-based composites using DIC, and obtained the evolution law of the surface displacement field and strain field of the specimen. Wu (Wu et al., 2011) used DIC technology to monitor the crack opening displacement during the concrete fracture process. The test results were found to be consistent with the extensometer results, thus verifying the reliability of using DIC technology to study the concrete fracture process.

The failure of materials under blast loads is usually dominated by the tensile failure of the back blast surface (Yang, 2020). Thus, it is necessary to study the dynamic tensile properties of macro-PPFRCCs. This paper reports the results of experiments in which the dynamic Brazilian splitting test was used to test cementitious composites with six different macro-polypropylene fiber (macro-PPF) volume fractions.

2 Materials and Methods

2.1 Materials

Considering the effect of excessively high dosages, where the fibers bind together to form agglomerates, the fiber volume fraction δ of the macro-PPF was selected to be 0%, 0.5%, 1%, 1.5%, 2%, and 2.5%. The fiber properties are listed in Table 1, and the mix proportions of the cementitious composite specimens are presented in Table 2.

A group of specimens with no added macro-PPF was used as a control group; this group is indicated by the prefix N-0. The different macro-PPFRCC groups are numbered as PP-*i*-*j*-*y*, where PP denotes that the specimen contains macro-polypropylene fiber; $i = 0.5$, 1, 1.5, 2, or 2.5 indicates the δ value of the fiber; $j = 3$, 4, 5, 6, or 7 corresponds to the impact velocity (m/s); and y is the test count. The Brazilian disc specimens used in the test and the Brazilian disc specimens after being sprayed with speckles are shown in Fig. 1.

2.2 SHPB Device and Dynamic DIC System

The dynamic splitting tensile test of macro-PPFRCC specimens was carried out using an SHPB with a diameter of 50 mm. A high-speed camera (Kirana-5 M) was used to collect pictures of the fracture process of the macro-PPFRCC specimens. During the experiments, the trigger mode was set to a falling edge trigger, and the trigger voltage was the same as that of the ultra-dynamic strain gauge. The acquisition rate, spatial resolution, and camera trigger time were set to 100,000 fps, 10.2 PPi/mm, and 0 μs, respectively. A schematic diagram of the test setup is shown in Fig. 2.

2.3 Test Data Processing

The loading force at both ends of the specimen can be obtained from

Table 2 Mix proportions of polypropylene fiber concrete

Number	Sand/ kg m^{-3}	Water/ kg m^{-3}	Cement/ kg m^{-3}	Fly ash/ kg m^{-3}	δ/%
N-0	541	303	649	433	0
PP-0.5	541	303	649	433	0.5
PP-1	541	303	649	433	1
PP-1.5	541	303	649	433	1.5
PP-2	541	303	649	433	2
PP-2.5	541	303	649	433	2.5

Table 1 Fiber properties

Fiber type	Diameter	Length	Tensile strength	Elastic modulus	Water absorption
Modified polypropylene fiber	0.18 mm	12 mm	750 MPa	8GPa	Does not absorb water

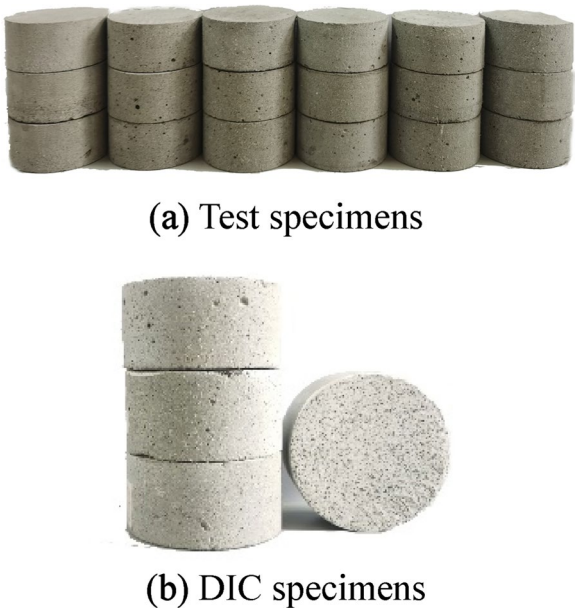

Fig. 1 Brazilian disc specimens

$$\left.\begin{aligned} P_1 &= AE(\varepsilon_i + \varepsilon_r) \\ P_2 &= AE\varepsilon_t \end{aligned}\right\} \tag{1}$$

where A and E are the cross-sectional area and elastic modulus of the bar, respectively. A schematic diagram of the dynamic tensile loading of a Brazilian disc specimen is shown in Fig. 3.

According to the Information Security Risk Management (ISRM) recommendations (Zhou, 2011), the dynamic force should be balanced. A dynamic force balance verification diagram is shown in Fig. 4. It can be seen that the dynamic force balance has been achieved.

The dynamic tensile stress $\sigma_T(t)$ of the macro-PPFRCC specimens can be obtained by Xie et al. (2022); Zhou, 2011)

$$\sigma_T(t) = \frac{2P(t)}{\pi BD} \tag{2}$$

where $P(t)$ is the load on the specimen and B, D are the thickness and diameter of the disc specimen, respectively.

2.4 Determination of Load Rate

According to the ISRM recommendations (Zhou, 2011), the loading rate $\dot{\sigma}$ is generally determined by the slope of the linear segment of the stress–time curve. The loading rate determination curve for a typical specimen in this study is shown in Fig. 5.

In this paper, five impact velocities (3 m/s, 4 m/s, 5 m/s, 6 m/s, and 7 m/s) were set, and each group of specimens was tested three times at each impact speed.

3 Results

3.1 Test Results

By analyzing the test results in this paper, there is a significant positive relationship between the dynamic tensile strength σ_T and the loading rate $\dot{\sigma}$. The typical experimental results are shown in Fig. 6.

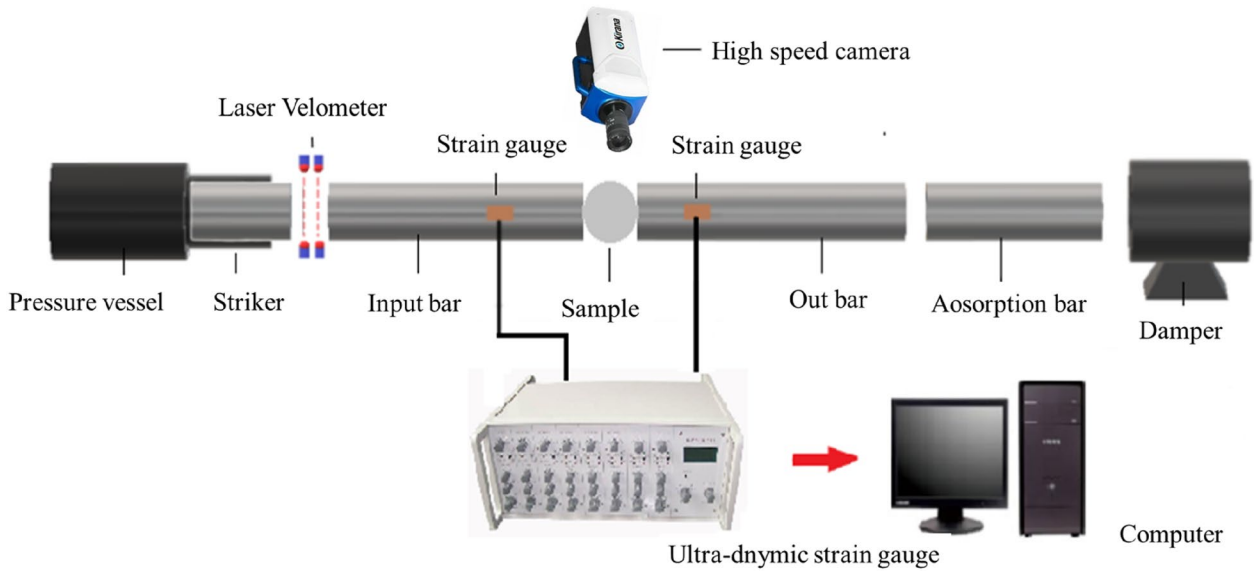

Fig. 2 Schematic diagram of the experimental setup

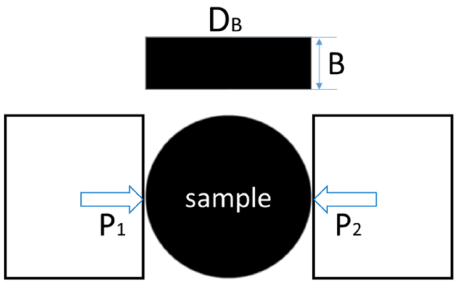

Fig. 3 Schematic diagram of dynamic stretching

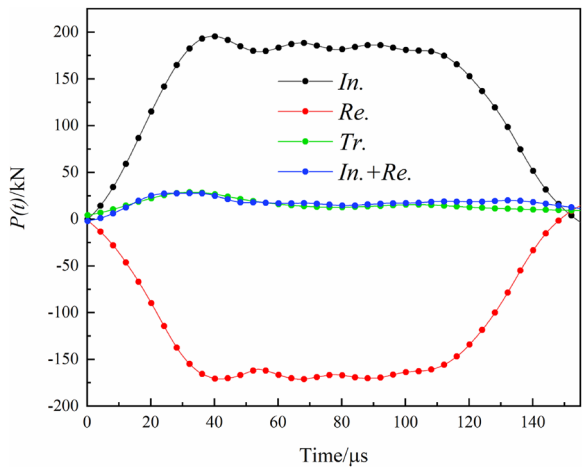

Fig. 4 Verification of force balance for a typical specimen

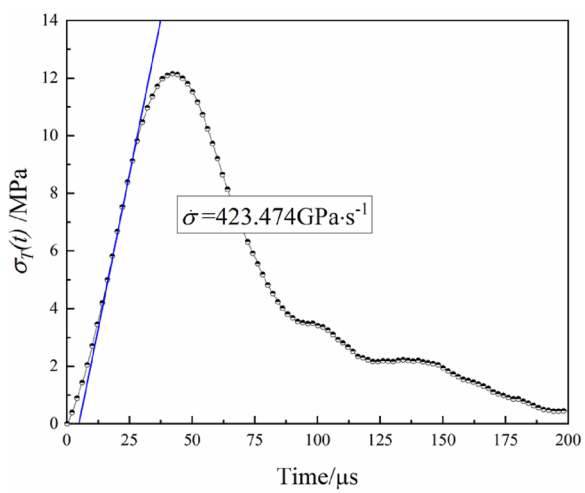

Fig. 5 Determination of loading rate of typical specimen

As can be seen from Fig. 6, when δ is less than 2%, the addition of macro-PPF creates a bonding effect between the matrix of the macro-PPFRCC specimen, preventing

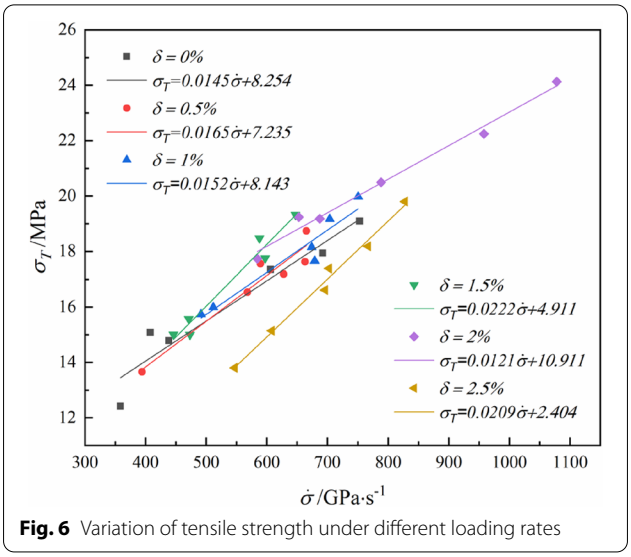

Fig. 6 Variation of tensile strength under different loading rates

and delaying the development of microcracks. Therefore, the dynamic tensile strength of the specimen is improved. When δ exceeds 2%, the addition of fibers negatively affects the strength because of the associated increase in porosity. When the loading rate is less than 650 GPa/s, the specimen with 1.5% macro-PPF exhibits relatively high strength, whereas when the loading rate exceeds 650 GPa/s, specimens with 2% macro-PPF have relatively high strength.

3.2 Dynamic Splitting Strength as a Function of Loading Rate and Fiber Volume Fraction

The results presented in Sect. "Test results" indicate that the strength σ_T of the macro-PPFRCC specimens is affected by two factors: the loading rate $\dot{\sigma}$ and the fiber volume fraction δ. Thus, the strength has a functional relationship of the form:

$$\sigma_T = f_t(\dot{\sigma}) + f_t(\delta) \tag{3}$$

where $f_t(\dot{\sigma})$ is the strength function related to $\dot{\sigma}$ and $f_t(\delta)$ is the strength function related to δ. According to Fig. 6, there is a linear relationship between σ_T and $\dot{\sigma}$, so $f_t(\dot{\sigma})$ can be written as

$$f_t(\dot{\sigma}) = K_1\dot{\sigma} + C_1 \tag{4}$$

Relevant research suggests that the strength of fiber cement-based composites does not always increase with increasing fiber content. When the fiber content becomes too high, the strength deteriorates because of fiber agglomeration (Ahmed et al., 2009), which causes a reduction in tensile strength. The experimental results also suggest that there is a nonlinear relationship

between σ_T and δ. As shown in Fig. 7, under the impact loads considered in this study, the tensile strength of the specimen increases and then decreases as δ increases, although the initial increase is not significant at lower fiber concentrations.

Therefore, there is a polynomial functional relationship between δ and $f_t(\delta)$ of the form:

$$f_t(\delta) = A\delta^3 + B\delta^2 + C\delta + C_2 \tag{5}$$

Equations (4) and (5) can be substituted into Eq. (3) to give the following expression for the tensile strength of macro-PPFRCC specimens:

$$\sigma = K_1\dot{\sigma} + A\delta^3 + B\delta^2 + C\delta + K_2 \tag{6}$$

where K_2 is the sum of the constant terms:

$$K_2 = C_1 + C_2 \tag{7}$$

To determine the parameters K_1, A, B, C, and K_2 in these equations, we use the undetermined coefficient method. The coefficients K_1 and K_2 can be obtained by linear fitting of the test results from specimens with a fiber volume fraction of 0%. These values can be substituted into Eq. (6) for simplification, and then the relationship between $f_t(\sigma)$ and δ can be obtained. The parameters A, B, and C are determined by fitting the cubic function relationship between $f_t(\sigma)$ and δ for each group of specimens under similar loading rates. The results are shown in Fig. 8.

Finally, we obtain the following expression for the dynamic tensile strength of the macro-PPFRCC specimens considered in this study:

$$\sigma = 0.0145\dot{\sigma} - 1.0957\delta^3 + 2.7804\delta^2 - 0.762\delta + 8.254 \tag{8}$$

Typical test points can be compared with the fitted curve in Fig. 7.

It can be seen from Fig. 9 that the fitting function has a high degree of correlation with the test results obtained in the experiments. Thus, this expression accurately reflects the influence of the fiber volume fraction and loading rate on the dynamic tensile strength of macro-PPFRCCs.

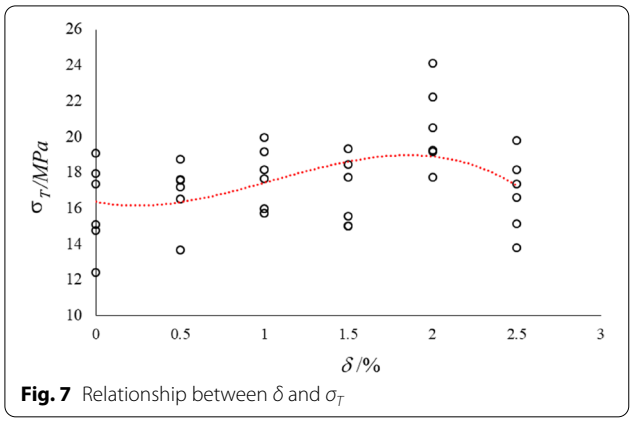

Fig. 7 Relationship between δ and σ_T

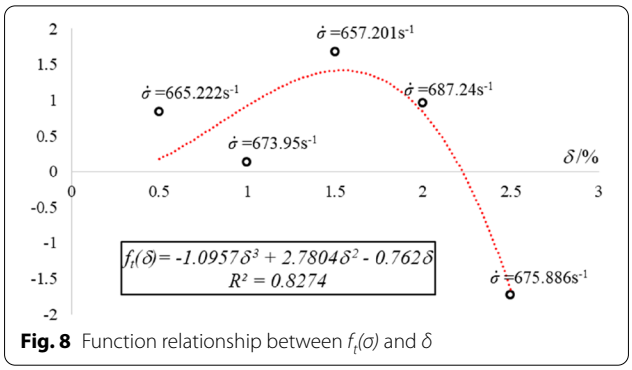

Fig. 8 Function relationship between $f_t(\sigma)$ and δ

4 Analysis of DIC Results

4.1 Fracture Process

To explore the failure mechanism of the macro-PPFRCC specimens, the failure process was recorded by a high-speed camera. Through image analysis, it is found that the fiber content significantly affects the crack initiation mode of the specimens. When $\delta = 0\%$ and 0.5%, the specimen cracks from the center. The typical crack initiation process of the specimen is shown in Fig. 10. As δ increases, the specimens crack from both ends; the typical crack initiation process for this case is shown in Fig. 11.

In splitting tests using cementitious composites, the homogeneity of the material has a significant effect on the crack initiation mode of the specimen (Xu et al., 2020; Yang et al., 2021). In this study, when δ is low

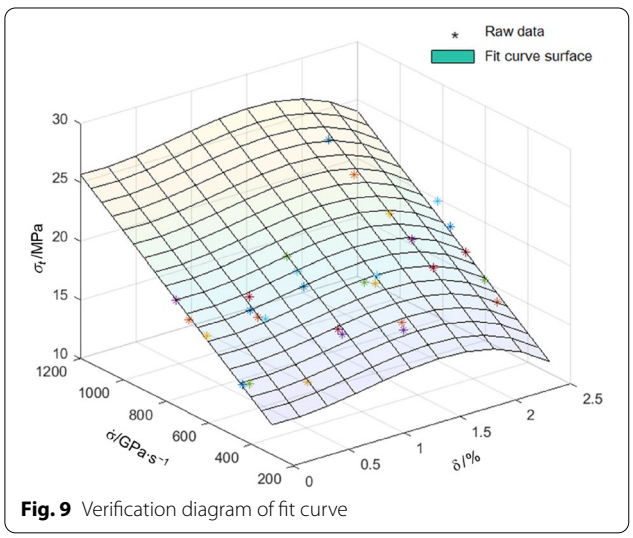

Fig. 9 Verification diagram of fit curve

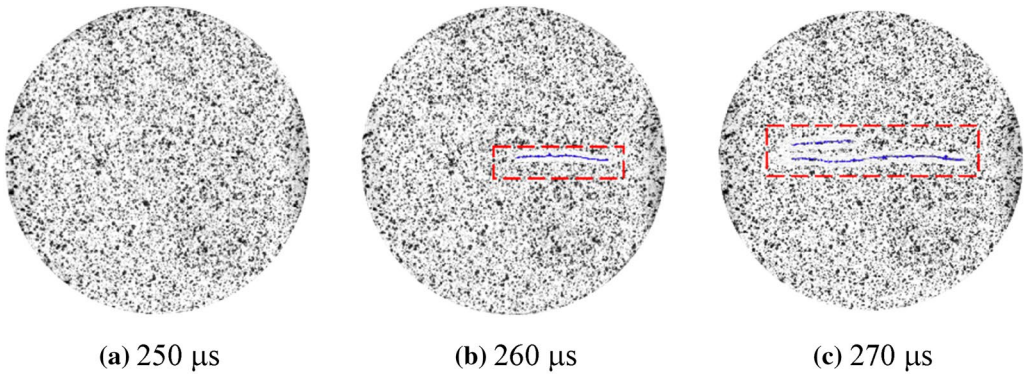

Fig. 10 Crack initiation in the center of the PP-0.5-3-1 specimen

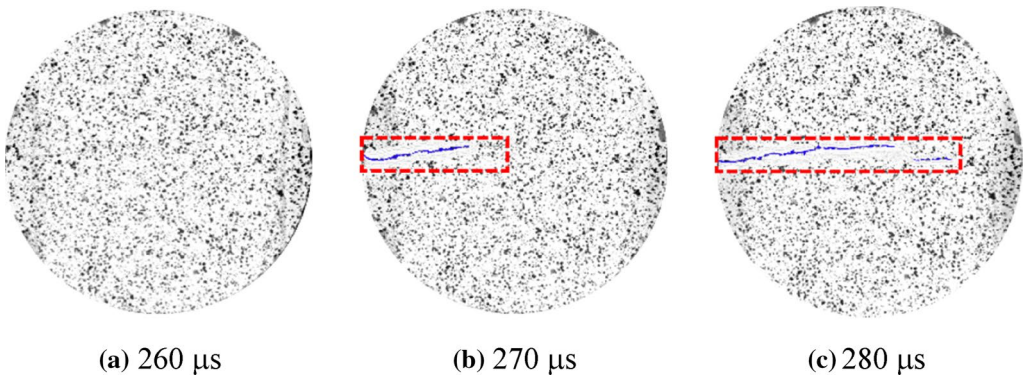

Fig. 11 Crack initiation at the end of PP-1.5-3-2 specimen

(0–0.5%), the porosity of the specimen is low and the material is relatively homogeneous, and so the material is prone to tensile failure in its center, where the tensile stress is most concentrated. With increasing fiber volume fraction, the tensile failure resistance of the specimen improves significantly, and so failure in the center of the specimen is avoided. However, as the porosity increases, the combined action of shear stress and tensile stress causes microcracks to develop in the area, where the specimen is in contact with the bar, and these microcracks propagate along the loading axis.

Further analysis of the dynamic splitting process was conducted using the VIC-2D software to postprocess the captured images. We selected a square area of the specimen as the area of interest (*AOI*), and placed one measuring point in every nine-pixel region on the center line (*ST* line) of the AOI. These measuring points

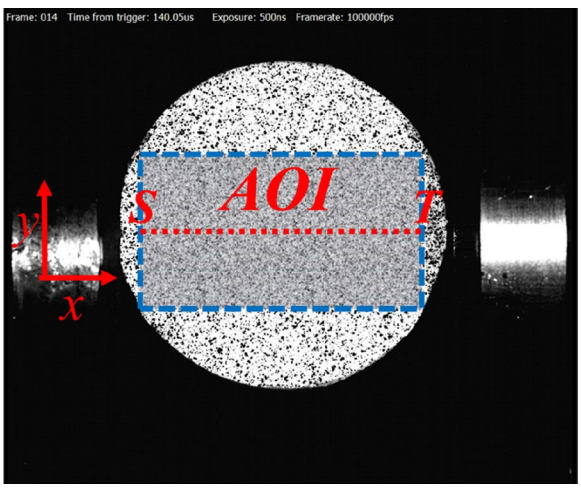

Fig. 12 DIC analysis area

were used to analyze the change in the displacement and strain fields of the specimen, as shown in Fig. 12.

The y-direction displacement field and a strain field evolution cloud map were calculated for each group of specimens. The results for two typical specimens are shown in Figs. 13 and 14.

Comparing the displacement field changes in Figs. 13 and 14, it can be seen that, initially, the distribution of the displacement field on the surface of the specimens is relatively uniform, and there are no significant changes in the displacement gradient. As the loading progresses, the displacement gradient changes in the AOI. The larger displacement gradient of specimen PP-0.5-3-1 is concentrated in the center of the specimen, while that of specimen PP-2-3-1 is concentrated in the area close to the right end of the bar. This phenomenon leads to the different crack initiation positions of this specimen. Similarly, by analyzing the variations in the strain fields in Figs. 13 and 14, it can be seen that before the specimens undergo crack initiation, there is no significant strain concentration in the AOI. As the loading progresses, the specimens begin to exhibit significant strain concentration along the loading axis. With the crack initiation, the strain begins to decrease, except at the crack initiation position, and the strain concentration phenomenon is released. The crack initiation position of specimen PP-0.5-3-1 is concentrated in the center of the AOI, while specimen PP-2-3-1 suffers crack initiation on its right side, where a flame-like strain concentration area appears, and the crack propagates along the loading axis.

The information obtained by DIC was further analyzed to obtain the changes in the tensile strain ε_y at each measuring point on the *ST* line for each group. The results for a typical specimen from each group at the same impact velocity (3 m/s) are shown in Fig. 15. In the figure, Δx is the distance of the measuring point from the left endpoint of the *ST* line.

As can be seen from Fig. 15a, b, the variation of ε_y at each measuring point on the *ST* line is relatively uniform. The increase in the strain at each point is relatively small, and the longitudinal strain distribution on the *ST* line is approximately straight. As the loading progresses, the curves at each time become approximately parallel. When the fiber volume fraction is relatively high, Fig. 15c–f shows that the strain on the *ST* line of each specimen does not vary evenly. The strain at the right measuring point of the *ST* line changes significantly faster than at the left measuring point, which affects the crack initiation position of the specimen. To further evaluate the tensile properties of the specimens with various volume fractions of macro-PPF, and accurately determine

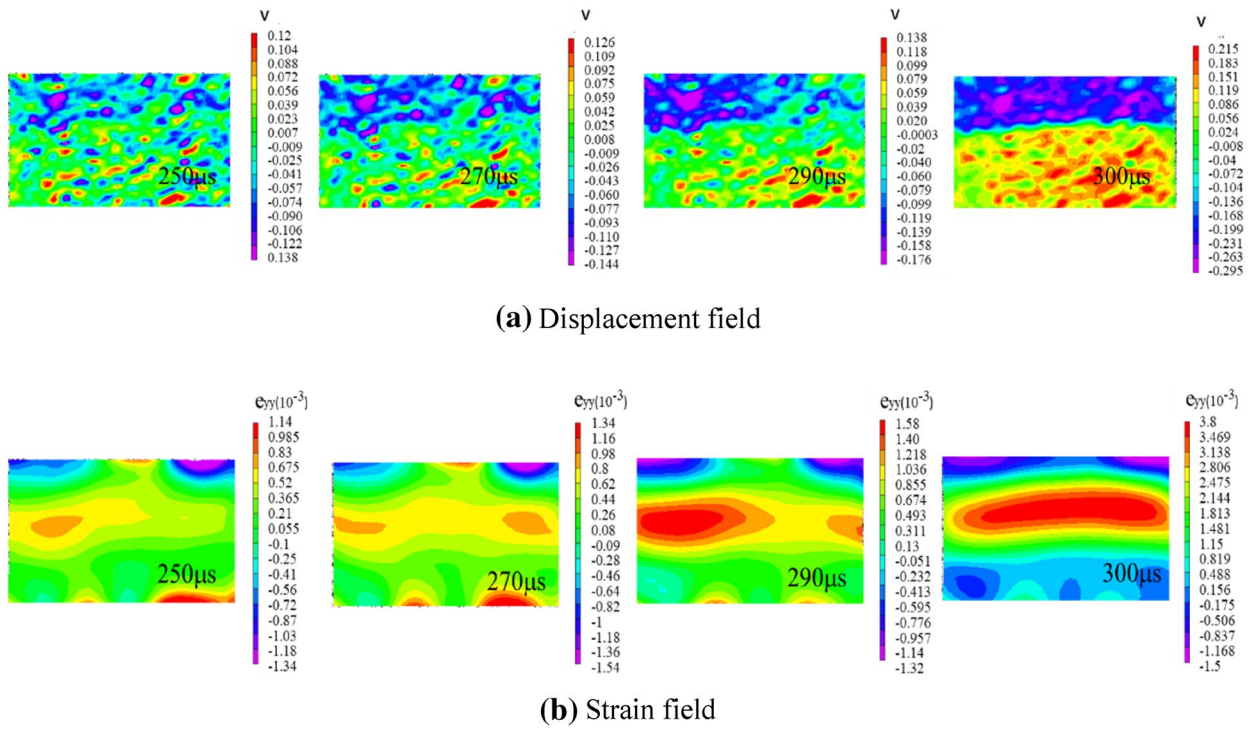

Fig. 13 DIC analysis results of PP-0.5-3-1

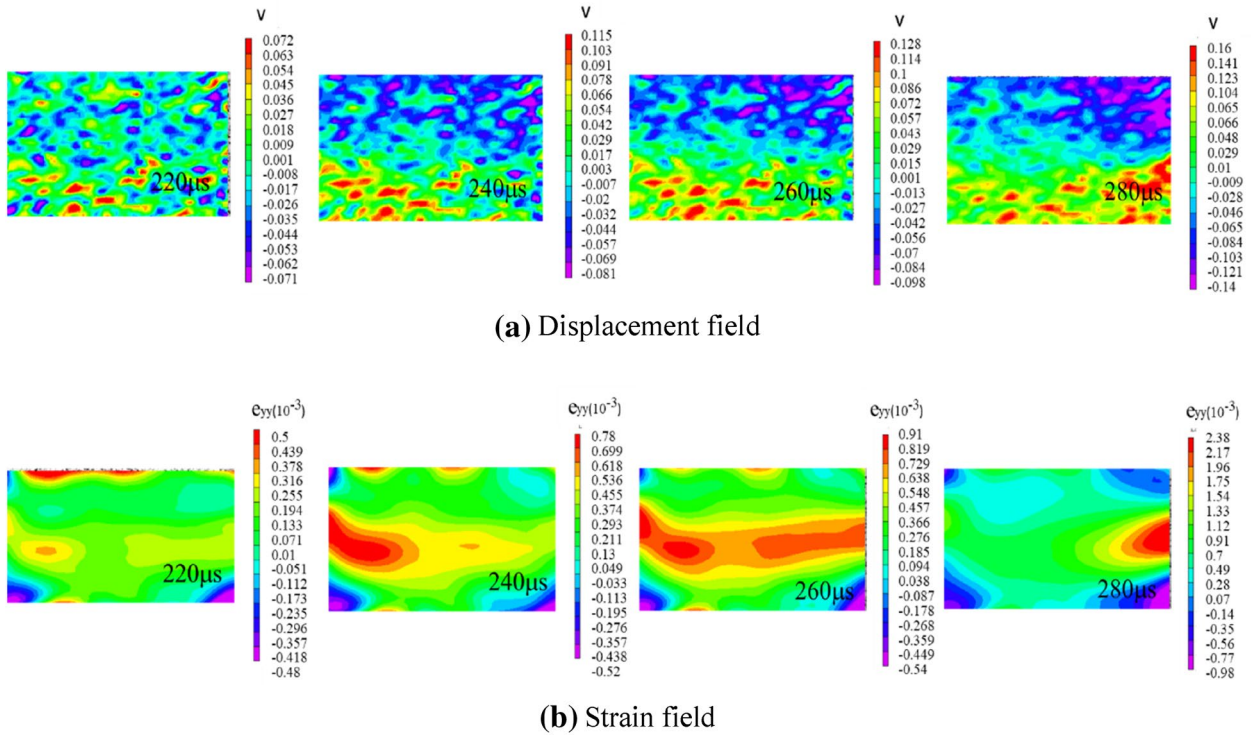

Fig. 14 DIC analysis results of PP-2-3-1

the crack initiation strain, the strain changes were analyzed at each measuring point on the *ST* line. Fig. 16 shows the evolution of ε_y at a typical measuring point on the *ST* line.

As can be seen from Fig. 16, during the initial loading period, the tensile strain at the measuring point exhibits a nonlinear change. With the initiation and propagation of microcracks, the nonlinearity of the curve reaches a maximum, and the specimen begins to exhibit macroscopic fractures. At this time, ε_y reaches the crack initiation strain, and the nonlinearity of the curve begins to weaken toward a linear change. To further quantify this change process, the curvature of the ε_y-t curve at each measuring point on the *ST* line at each moment is shown in Fig. 17. To ensure uniform order of magnitude in the numerator and denominator when calculating the curvature, the strain and time units were set to 10^{-3} and 10 μs, respectively.

Fig. 17 shows that the curvature of the ε_y-t curve accurately quantifies the variations in ε_y. Greater values of the curvature indicate a higher degree of nonlinearity of the strain curve at that location. A decrease in the curvature indicates that the degree of nonlinearity is decreasing. As the curvature approaches 0, the changes become linear. In this paper, the tensile strain corresponding to the moment at which the degree of nonlinearity begins to decrease is taken as the crack initiation strain, that is, the value corresponding to the moment after the curvature has peaked. Fig. 17 also shows that the propagation process of the crack evolves, and the peak points at each measuring point do not all occur at the same time. Therefore, to avoid errors, the average value of the crack initiation strain obtained at each measuring point on the *ST* line is taken as the crack initiation strain ε_t of the specimen.

According to the results obtained in this study, there is no significant correlation between the crack initiation strain of the specimen and the impact velocity. Under the same fiber volume fraction, the crack initiation strain of the specimen fluctuates within a small range. The average value of ε_t for each group of specimens is shown in Fig. 18.

As can be seen from Fig. 18, when δ is in the range 0–1%, ε_t increases significantly with respect to δ, indicating that the addition of macro-PPF significantly improves the ability of the specimen to control crack development. When δ exceeds 1%, the ability to control cracking becomes limited. The ε_t values of specimens with $\delta = 1\%$, 1.5%, and 2% fluctuates in a similar range, indicating that an increase in δ also enhances the porosity of the specimen. When δ is greater than 2%, the crack initiation strain of the specimen decreases

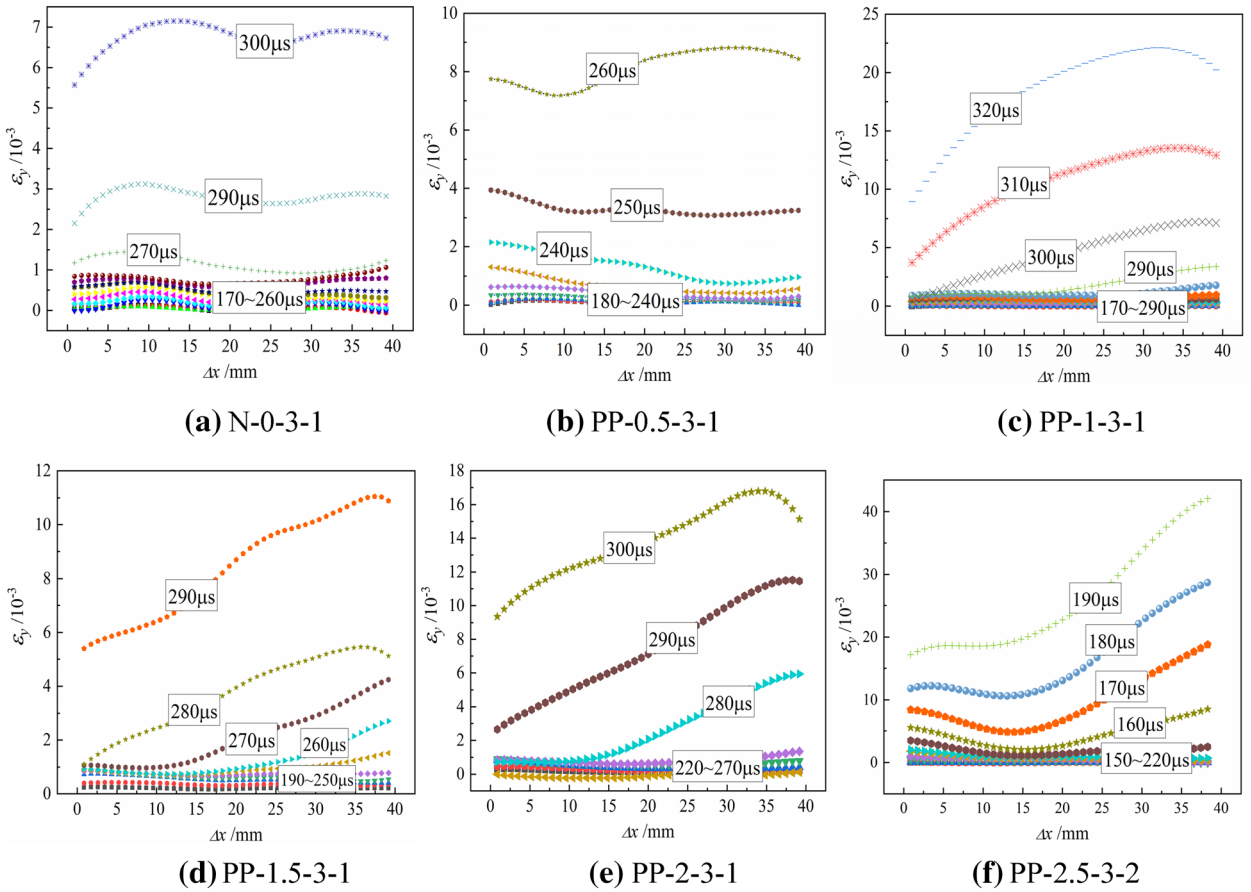

Fig. 15 Strain on ST line of each group of specimens under impact velocity of 3 m/s

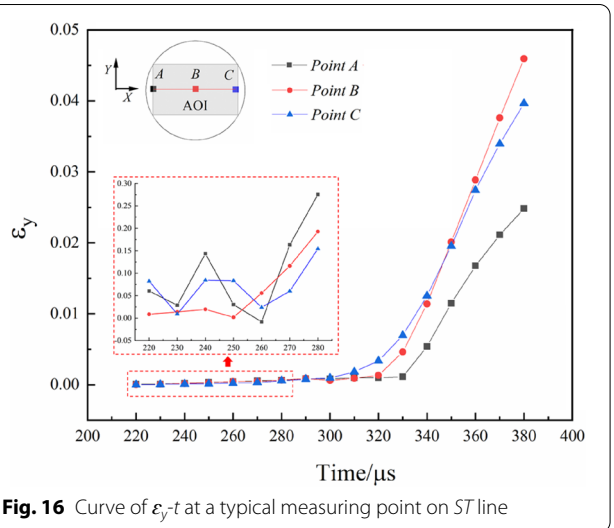

Fig. 16 Curve of ε_y-t at a typical measuring point on *ST* line

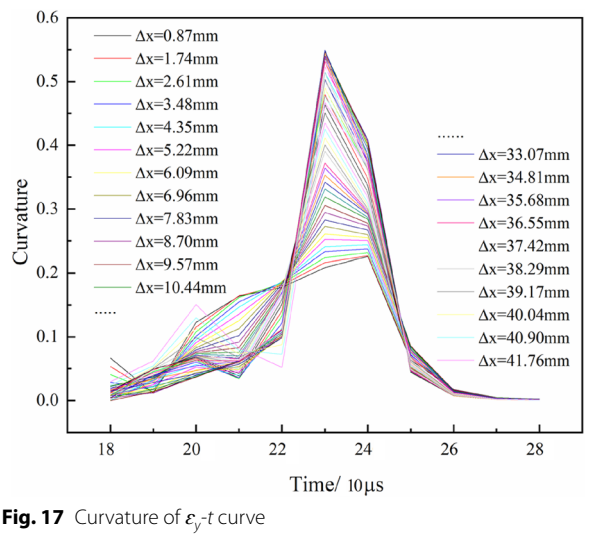

Fig. 17 Curvature of ε_y-t curve

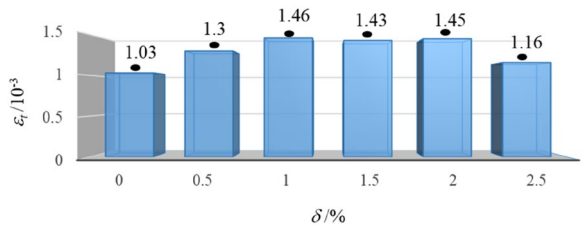

Fig. 18 Relationship between ε_t and fiber volume fraction

significantly. Combined with the analysis of the tensile strength presented in this paper, the appropriate fiber content (such that the cement cracks, but the fibers do not break) allows the specimen to retain some bearing capacity. Brittle failure transforms into ductile failure, and the specimens exhibit good strain hardening characteristics, so their strength has improved.

4.2 Failure Mode

The failure modes of typical specimens are presented in Table 3.

It can be seen from Table 3 that the failure modes of specimens with different fiber volume fractions have significant differences. Compared with the specimen with no added fibers, the macro-PPFRCCs are in fewer fragments after failure, and the shape remains relatively complete. Under low-speed impact, a crack basically develops along the central axis of the specimen. As the impact velocity increases, the number of cracks in the specimen increases, and the specimen breaks into more pieces. Compared with the complete cracking of specimens with fiber volume fractions of 0–1.5%, specimens with fiber volume fractions of 2–2.5% exhibit relatively few cracks under the same impact velocity. This phenomenon shows that the fibers play a good role in connecting the material

Table 3 Failure modes of macro-PPFRCCs

Fiber volume fraction	Impact velocity				
	3 m/s	4 m/s	5 m/s	6 m/s	7 m/s
0%					
0.5%					
1%					
1.5%					
2					
2.5					

matrix and improving the integrity of the specimen. This improves the impact resistance of the specimens and prevents tensile damage.

5 Conclusions

To explore the influence of the fiber volume fraction and loading rate on the dynamic tensile strength and failure mechanism of macro-PPFRCCs, the dynamic Brazilian splitting test was applied to cementitious composites with six different macro-PPF volume fractions (0%, 0.5%, 1%, 1.5%, 2%, and 2.5%). The following conclusions have been obtained:

(1) The incorporation of fibers has both positive and negative effects. When the added macro-PPF exceeds 2% by volume, the fibers negatively affect the strength, resulting in deterioration of the specimen because of the associated increase in porosity.

(2) Both the loading rate and the fiber content have significant effects on the strength of the specimen. The dynamic tensile strength of macro-PPFRCCs can be determined as a function of these two factors. Under the experimental conditions of this paper, the relationship was found to be as follows:

$$\sigma_T = 0.0145\dot{\sigma} - 1.0957\delta^3 + 2.7804\delta^2 - 0.762\delta + 8.254$$

(3) The volume fraction δ of macro-PPF significantly affects the crack initiation mode of the specimen. When $\delta = 0$–0.5%, the specimen cracks from the center. An increase in δ leads to microcracks developing in the area, where the specimen is in contact with the bar. A reasonable amount of fiber prevents the specimen from being damaged by central tension under dynamic loading, and distributes the impact load more evenly.

(4) Adding macro-PPF improves the ability of the specimen to resist cracking. An appropriate fiber content can significantly increase the crack initiation strain of the specimen.

Acknowledgements
We thank Stuart Jenkinson, PhD, from Liwen Bianji (Edanz) (www.liwenbianji.cn/) for editing the English text of a draft of this manuscript.

Author contributions
YG: conceptualization, funding acquisition, writing—review and editing. BJ: conceptualization, data curation, writing—original draft, methodology, writing—review and editing. DZ: data curation. LY: investigation. LY: investigation. All authors read and approved the final manuscript.

Author information
Guoliang Yang, Associate Professor, School of Mechanics and Architectural Engineering, China University of Mining and Technology (Beijing), Beijing 100083, China. Email: yanggl531@163.com. Jingjiu Bi, PhD Student, School of Mechanics and Architectural Engineering, China University of Mining and Technology (Beijing), Beijing 100,083, China. Email: bijingjiu@126.com. Zhiwen Dong, PhD Student, School of Mechanics and Architectural Engineering, China University of Mining and Technology (Beijing), Beijing 100083, China. Email: 962113845@qq.com. Ying Li, Master's Student, School of Mechanics and Architectural Engineering, China University of Mining and Technology (Beijing), Beijing 100083, China. Email: liying@student.cumtb.edu.cn. Yi Liu, Master's Student, School of Mechanics and Architectural Engineering, China University of Mining and Technology (Beijing), Beijing 100083, China. Email: 1027697890@qq.com.

Funding
There are no funders to report for this submission.

Availability of data and materials
All data generated or analyzed during this study are included in this published article [and its supplementary information files].

Declarations

Competing interests
The authors declare that they have no known competing financial interests or personal relationships that could have appeared to influence the work reported in this paper.

Received: 27 June 2022 Accepted: 7 September 2022
Published online: 05 December 2022

References

Ahmed, S., et al. (2009). Tensile strain hardening behaviour of hybrid steel-polyethylene fiber reinforced cementitious composites. *Construction and Building Materials, 23*(1), 96–106.
Enrico, W., et al. (2021). Dynamic single-fiber pull-out of polypropylene fibers produced with different mechanical and surface properties for concrete reinforcement. *Materials, 14*(4), 722.
Guo, H., et al. (2019). Effect of steel and polypropylene fibers on the quasi-static and dynamic splitting tensile properties of high-strength concrete. *Construction and Building Materials, 224*, 504.
Hsie, M., et al. (2008). Mechanical properties of polypropylene hybrid fiber-reinforced concrete. *Materials Science & Engineering A, 494*(1–2), 153.
Konstantinos, T., & Pantazopoulou, S. J. (2021). Bond behavior of high-performance fiber reinforced concrete (HPFRC) under direct tension pullout. *Engineering Structures, 243*, 112701.
Liang, N. H., et al. (2018). A study on dynamic compressive mechanical properties of multi-size polypropylene fiber concrete under high strain rate. *Mater Rev, 32*(1), 288–294.
Liang, N. H., et al. (2022). Experimental investigation on the mechanical properties of polypropylene hybrid fiber-reinforced roller-compacted concrete pavements. *InternationalJournal of Concrete Structures and Materials*. https://doi.org/10.1186/s40069-021-00493-6
Mazaheripour, H., et al. (2010). The effect of polypropylene fibers on the properties of fresh and hardened lightweight self-compacting concrete. *Construction and Building Materials, 25*(1), 351–358.
Niu, Y. F., et al. (2019). Development of the strain field along the crack in ultra-high-performance fiber-reinforced concrete (UHPFRC) under bending by digital image correlation technique. *Cement and Concrete Research, 125*, 105821.
Pakravan, H. R., Latifi, M., & Jamshidi, M. (2017). Hybrid short fiber reinforcement system in concrete: A review. *Construction and Building Materials, 142*, 280.
Qing, L. B., et al. (2019). Experimental investigation of the concrete permissible damage scale based on the digital image correlation method. *Eng Mech, 36*(10), 115–121.
Wu, Z. M., et al. (2011). An experimental investigation on the FPZ properties in concrete using digital image correlation technique. *Engineering Fracture Mechanics, 78*(17), 2978.
Xie, H. Z., et al. (2022). Research on energy dissipation and damage evolution of dynamic splitting failure of basalt fiber reinforced concrete. *Construction and Building Materials, 330*, 127292.
Xu, J. P., et al. (2020). Experimental analysis of process and tensile strength for concrete brazilian splitting test with different loading boundaries by DIC method. *Chinese Journal of Theoretical and Applied Mechanics, 52*(03), 864–876.

Yang, G. L., et al. (2020). Antiexplosion Performance of Engineered Cementitious Composite Explosion-Proof Wall. *Advances in Materials Science and Engineering, 2020*, 1.
Yang, R. Z., et al. (2021). Experimental study on dynamic mechanics, energy characteristics, and failure mechanism of Rubber Cement Mortar under SHPB splitting test. *Materials Reports, 35*(10), 10062–10072.
Yin, S., et al. (2015). Use of macro plastic fibres in concrete: A review. *Construction and Building Materials, 93*, 180.
Yu, K. Q., et al. (2018). Development of ultra-high performance engineered cementitious composites using polyethylene (PE) fibers. *Construction and Building Materials, 158*, 217.
Zhao, Y., et al. (2018). Impact damage characteristics of steel fiber reinforced cement matrix composites based on digital image correlation. *Acta Materiae Compositae Sinica, 35*, 1325.
Zhong, Z., et al. (2018). Steel fiber-reinforced concrete under impact loading dynamic constitutive equation. *Construction and Building Materials, 190*, 1049.
Zhou, Y. X., et al. (2011). Suggested methods for determining the dynamic strength parameters and mode-I fracture toughness of rock materials. *International Journal of Rock Mechanics and Mining Sciences, 49*, 105.

Publisher's Note